Comparative Analysis of Lipid Composition and Thermal, Polymorphic, and Crystallization Behaviors of Granular Crystals Formed in Beef Tallow and Palm Oil

Zong Meng, Yuan-Fa Liu, Qing-Zhe Jin, Jian-Hua Huang, Zhi-Hua Song, Feng-Yan Wang, and Xing-Guo Wang*

State Key Laboratory of Food Science and Technology, School of Food Science and Technology, Jiangnan University, 1800 Lihu Road, Wuxi 214122, Jiangsu Province, People's Republic of China

ABSTRACT: Six rectangular block all beef tallow (BT)-based and all palm oil (PO)-based model shortenings prepared on a laboratory scale, respectively denoted BTMS and POMS, were stored under temperature fluctuation cycles of 5−20 °C until granular crystals were observed. The lipid composition and thermal, polymorphic, and isothermal crystallization behaviors of the granular crystals and their surrounding materials separated from BTMS and POMS, respectively, were evaluated. The changes of nanostructure including the aggregation of high-melting triacylglycerols (TAGs) and polymorphic transformation from β' form of double chain length structures to complicated crystal structures, in which the β and β' form crystals of triple and double chain length structures simultaneously coexist, had occurred in granular crystals compared with surrounding materials, whether in BTMS or in POMS. Consequently, a slower crystallization rate appeared in granular crystal parts of both model shortenings noted above, which would yield larger and fewer crystals indicated by the Avrami model analysis that would further aggregate to form large granular crystals.

KEYWORDS: Beef tallow, palm oil, granular crystals, triacylglycerols, polymorphism, crystallization behavior

■ INTRODUCTION

Beef tallow (BT), a byproduct of beef production, is an important animal fat extensivly used in bakery shortening and margarine manufacturing due to its advantageous properties, such as (i) high thermal and oxidative stability and (ii) unique desirable flavor after baking. Palm oil (PO) has also been a prominent fat and oil resource for vegetable oil-based fat products, due to its *trans*-free characteristic, plasticity, heat stability, and price competitiveness. However, the use of BT or PO for solid fats in plastic fat products has encountered serious structural defects in the formation of granular crystals in shortenings and margarines, which impair the consistency and plasticity of fat products. These granular crystals, with diameters of 0.1−3 mm or even bigger, are easily formed during handling, storage, and transportation of BT/PO-based shortenings and margarines, which can be detected by consumers by rubbing the fat between the fingers or when the fat is melted in the mouth.[1,2] Thus, the understanding and control of granular crystal formation in high-fat formulations are very important points in the specialty fat industry.

The formation of granular crystals in PO-based fat blends has been investigated by several groups.[3−7] The β polymorph might be one reason for the formation of granular crystals in PO-based margarines.[3] In a model fat blend consisting of 1,3-dipalmitoyl-2-oleoylglycerol (POP) and rapeseed oil, reproduced granular crystals showed higher POP content than their surrounding materials, and the most stable β_1 polymorph of POP was observed to contribute to the formation of granular crystals.[4] In the margarines produced with excess palm oil, granular crystals showed POP as one of its major TAGs,[5] and TAG species such as

tripalmitin (PPP) and POP were related to texture degradation.[6] In a model margarine system composed of palm oil and PPP, the agglomeration of high-melting TAGs was found to lead to the formation of granular crystals.[7] Only our team studied the granular crystals in BT-based shortening, suggesting that the agglomerates of high-melting TAGs with simultaneous transformation to the more stable β crystal polymorph and, concomitantly, a slower crystallization rate with an increase in crystal growth led to the formation of large crystals and further aggregated to larger granular crystals.[1,2] According to these studies, however, the fundamental question of how the granular crystals formed in PO-based plastic fats on the micrometer scale were connected with the TAGs and polymorphisms on the molecular scale is still unclear. Moreover, to date, attempts have not yet been made regarding the comparative analysis of the formation mechanism of granular crystals in BT and PO. The exact mechanism of the formation of granular crystals in BT/PO-based shortenings and margarines is still to be illuminated. To fully understand the crystallization behavior of BT/PO and their role in the formation of granular crystals in BT/PO-based plastic fats, the structure hierarchy of granular crystals formed in BT and PO, which is structured by an underlying fat crystal network must be clarified.

Within this framework, in the present study granular crystals were reproduced in BTMS and POMS, respectively. Following

the structure hierarchy of fat crystal networks, the lipid composition, thermal properties, polymorphism, and crystallization behavior of granular crystals and their surrounding materials were examined systematically in a comparative study. Therefore, the present study may be able to give a better understanding of the similarities and differences of the mechanism causing the formation of granular crystals in BT/PO-based plastic fat products.

■ MATERIALS AND METHODS

Materials. Refined, bleached, and deodorized (RBD) BT (iodine value (IV) = 45.15 g of I_2/100 g and slip melting point (SMP) = 44.5 °C) and PO (IV = 52.87 g of I_2/100 g and SMP = 34.6 °C) were produced and generously donated by Kerry Specialty Fats Ltd. (Shanghai, China). These two kinds of fats are widely used in animal fat-based and vegetable oil-based plastic fat products in China, respectively. Supelco 37 Component FAME Mixture was purchased from Sigma-Aldrich China (Shanghai, China). All other reagents and solvents were of analytical or chromatographic grade purchased from Sinopharm Chemical Reagent Co. Ltd. (Shanghai, China) to suit analytical requirements.

SMP. The SMP was determined according to AOCS standards, method Cc 3-25.[8] Briefly, fat filled up to 1 cm in open capillary tubes was presolidified by touching over a piece of ice and then chilled at 10 ± 1 °C for 16 h. Three capillaries were attached gently to a thermometer using a rubber band before being immersed in a beaker of cold distilled water. The water was stirred and heated, and the temperature was recorded when the fat column began to rise in the tubes. Triplicate measurements were made, and the average value is reported above.

Preparation of Model Shortenings. The model "shortenings" were prepared according to the modified method of Braipson-Danthine and Deroanne.[9,10] About 1400 g of the melted fats (BT and PO, respectively) contained in the 2000 mL beaker were kept in an oven at 80 °C for 30 min to erase the crystal memory. Divided into six copies, each sample of 200 g was placed in one of six small rectangular block plastic vessels ($8 \text{ cm} \times 7 \text{ cm} \times 5 \text{ cm}$), respectively, and kept in liquid form at 45 °C with gentle stirring for 30 min. They were then put in a freezer at −20 °C for another an hour to simulate, on a laboratory scale, an industrial scraped surface heat exchanger. The fat samples were subsequently stored at room temperature (25 ± 1 °C) for 48 h. Then, six model BT-based and PO-based shortenings were obtained, respectively, and denoted BTMS and POMS.

Induction of Granular Crystals in Model Shortenings. Just after the shortenings had been produced, three model samples above were subjected to temperature cycling storage in a KBF115 programmable oven (Binder, Tuttlingen, Germany) in which the temperature was held at 5 °C for 12 h and at 20 °C for another 12 h, until granular crystals were observed visually. These induction procedures were performed in duplicate.[4,5] About 15 g of granular crystals (diameter ∼ 2−3 mm) was picked out from the inside of each shortening by tweezers and placed into the sample cell. All operations were performed at 20 °C, in a temperature-controlled room to reduce the risk of melting the granular crystals. A portion (∼3−4 g) of granular crystals was subjected to both fatty acid and TAG compositions analyses; and the other portion (∼11−12 g) was maintained in its original state at 5 °C for 24 h and then characterized by differential scanning calorimetry (DSC), X-ray diffraction (XRD), and pulsed nuclear magnetic resonance (pNMR) analyses. For comparison, the materials (∼15 g) surrounding the granular crystals were also analyzed in terms of all the above-mentioned indices.

Fatty Acid Composition. Fatty acid methyl esters (FAMEs) were prepared according to AOCS Official Method Ce 2-66[8] and subsequently analyzed with GC-14B gas chromatography (GC) equipped with a flame ionization detector (Shimadzu, Tokyo, Japan) and a fused-silica capillary column (CP-Sil88, 100 m × 0.25 mm × 0.2 mm). The temperature of the injection port and detector were both set

at 250 °C. The column was heated to 120 °C, held for 3 min, then programmed at 8 °C/min to 175 °C and held for 28 min, and then increased to 215 °C at 3 °C/min and held for 20 min. The fatty acid species were identified using the retention time of a FAME standard solution.

TAG Composition. TAGs were separated by reversed-phase high-performance liquid chromatography (HPLC) with a Waters 1525 binary pump (Milford, MA). Samples were dissolved in chloroform at a concentration of 5.0 mg/mL, and 5 μL was injected into a Nova-pak RP-C18 column (150 mm × 4.6 mm, particle size = 4 μm) (Waters). The column was kept at 35 °C. Acetonitrile/dichloromethane (65:35, v/v) as the eluent at a flow rate of 1.0 mL/min and a Waters 2424 evaporative light scattering detector (ELSD) were used. The drift tube temperature and the pressure of high-purity nitrogen nebulizer gas were 80 °C and 30 psi, respectively. TAGs were identified by high-performance liquid chromatography–atmospheric pressure chemical ionization mass spectrometry (HPLC/APCI-MS). The HPLC conditions were same as described before. A Platform ZMD 4000 (Waters) mass spectrometer (MS) equipped with an APCI interface was run at an APCI source block and probe temperature of, respectively, 100 and 400 °C and an MS multiplier voltage of 700 V. The measurement range was between m/z 250 and 1200. Qualitative and quantitative determinations of individual TAGs in fat blends were performed following the procedures of Liu et al.[11] and Chen et al.[12]

DSC. The thermal properties of the samples were measured using a Mettler Toledo DSC 1 (Mettler Toledo, Schwerzenbach, Switzerland). Samples (∼0.8 mg) were hermetically sealed in an aluminum pan with an empty pan serving as a reference. The samples were held at −40 °C for 5 min, and the melting profile was obtained by heating to 80 at 5 °C/min. After holding for 5 min at this temperature to remove completely the previous crystal structure, the crystallization profiles were obtained by cooling to −40 at 5 °C/min.

Crystal Polymorphism by XRD. The polymorphic forms of fat crystals in the blends were determined by D8 Advance XRD (Bruker, Karlsruhe, Germany), using Cu Kα radiation with Ni filter (k = 1.54056 Å; voltage, 40 kV; current, 40 mA; fixed 1.0, 1.0, and 0.1 mm divergence, antiscatter, and receiving slits, respectively). Samples were scanned from 1 to 30° (2θ scale), and the scan rate was set at 2°/min. The analyses were performed at ambient temperature. The short spacing of the α form appears near 4.15 Å, that of the β' form at 4.2 and 3.8 Å, and that of the β form at 4.6 Å (single strong spacing). β and β' type crystal contents in the samples were calculated from normalized areas by sum of peak areas. The areas were calculated by removing the background. The β form was calculated from the area of the short spacing at 4.6 Å, and the β' form was calculated from the areas of the short spacings at 4.2 and 3.8 Å using the formula

$$\%\beta = (A_\beta \times 100)/(A_\beta + A_{\beta'}); \quad \%\beta' = (A_{\beta'} \times 100)/(A_\beta + A_{\beta'})$$

where A_β and $A_{\beta'}$ were the peak areas of β and β' polymorphs, respectively.[13]

pNMR. Solid fat content (SFC) was measured by pNMR using a Bruker PC120 series NMR analyzer (Bruker). The water bath based cooling used in the pNMR experiments also offered rapid cooling and accurate temperature control. The instrument was automatically calibrated using three standards (supplied by Bruker) containing 0, 31.3, and 74.6% solid. Samples were run in triplicate, and the values were averaged. The SFC of the samples was determined using the following thermal treatment: NMR tubes were filled with the melted fat sample (about 2.5 g), kept at 80 °C for 30 min, and then placed in a thermostated water bath at 5, 10, 15, 20, 25, 30, and 35 °C; SFC readings were obtained at appropriate time intervals.

Avrami Model. pNMR data were fitted to the Avrami equation for isothermal crystallization. The Avrami equation can be used to quantify crystallization kinetics and give an indication of the nature of the crystallization

process, including nucleation and growth. It has the form

$$-\ln(1-f) = Kt^n \tag{1}$$

where f is the fraction of crystal transformed at time t during crystallization, K is the crystallization rate constant, which depends primarily on crystallization temperature, and n, the Avrami exponent, is a constant relating to the dimensionality of the transformation. The values of K and n are calculated from the intercept and slope, respectively, by the linear form of the Avrami equation as follows:

$$\ln[-\ln(1-f)] = n\ln t + \ln K \tag{2}$$

The numerical value of K is directly related to the half-time of crystallization, $t_{1/2}$, and therefore the overall rate of crystallization,[14] which is given by the following equation:

$$(t_{1/2})^n = 0.693/K \tag{3}$$

Statistical Analysis. Triplicate analyses ($n = 6$ for granular crystals and surrounding materials, respectively, whether in BTMS or in POMS) were performed for each dependent variable (fatty acid composition, TAG composition, thermal property, crystal polymorphism, and SFC). Analysis of variance (ANOVA) with Duncan's multiple-range test was carried out by Statistical Analysis System software (SAS, Cary, NC). Differences were considered to be significant at $P < 0.05$, and values of the means of triplicates $\pm$ standard deviations are presented.

■ RESULTS AND DISCUSSION

Lipid Composition. The fatty acid compositions of BT, PO, and the granular crystals and surrounding materials separated from BTMS and POMS, respectively, are given in Table 1. These results agree with BT and PO fatty acid ranges published in the literature.[15] The major fatty acids of granular crystals and surrounding materials in BTMS were palmitic acid ($C_{16:0}$, 26.15 and 25.25%, respectively), stearic acid ($C_{18:0}$, 20.67 and 19.48%, respectively), and oleic acid ($C_{18:1}$, 33.15 and 33.93%, respectively). In POMS, the predominant fatty acids of granular crystals and surrounding materials were $C_{16:0}$ (48.95 and 41.62%, respectively), $C_{18:1}$ (35.21 and 38.65%, respectively), and linoleic acid ($C_{18:2}$, 7.64 and 11.98%, respectively). Whether in BTMS or in POMS, the granular crystals and surrounding materials showed the same variation regularity in fatty acid compositions. That is, the former contained a little higher content of major high-melting saturated fatty acids ($P < 0.05$), for example, $C_{16:0}$ and $C_{18:0}$, and a little lower content of low-melting unsaturated fatty acids and minor saturated fatty acids ($P < 0.05$), for example, $C_{18:1}$, $C_{18:2}$, α-linolenic acid ($C_{18:3}$, omega-3 fatty acid), lauric acid ($C_{12:0}$), and myristic acid ($C_{14:0}$). Thus, concomitantly, the granular crystals contained 51.81 and 54.94% of the total saturated fatty acids (ΣSFA), higher than the surrounding materials of 49.91 and 47.48% ($P < 0.05$), respectively. Meanwhile, the former, contained 38.43 and 43.12% of the total unsaturated fatty acids (ΣUSFA), lower than the latter of 39.76 and 51.10% ($P < 0.05$), respectively. The implication was that high-melting SFA, for example, $C_{16:0}$ and $C_{18:0}$, had likely been linked with the structural defects of the plastic fats, as reported by other researchers.[7] Trans fatty acids (TFA) were reported to decrease the level of structural order of the crystals and also impart a certain faster crystallization and smaller crystals to the fat.[16] However, the small differences ($P < 0.05$) in the total TFA (ΣTFA) between the granular crystals and the surrounding materials in BTMS are essentially negligible, which may not fully support the major crystal structure differences between them.

Table 2 shows the TAG compositions of BT, PO, and the granular crystals in BTMS and POMS as well as the surrounding materials and their melting points.[17,18] These TAG compositions are also in accordance with BT and PO TAG ranges published in the literature.[11,19] For BTMS, the contents of higher melting TAGs, that is, PPP, POS, PPS, SOS, PSS, and SSS, in granular crystals were increased by 2.34, 11.26, 20.19, 30.55, 15.12, and 90.63%, respectively, whereas those of lower melting TAGs, that is, PLO, OOO, POO, POP, and SOO/SSL, were reduced by 1.18, 6.42, 19.53, 4.81, and 19.78%, respectively, compared with their surrounding materials ($P < 0.05$). For POMS, in particular, the percentage increase of higher melting POP, PPP, and POS TAGs in granular crystals reached 135.17, 30.99, and 80.36%, respectively; for lower melting PLO, PLP, OOO, POO, and SOO TAGs, on the contrary, 60.84, 51.95, 61.78, 57.21, and 79.33% reductions, respectively, compared with surrounding materials ($P < 0.05$) were detected. In addition, PPS and SOS contents declined substantially (a decrease of 70.00% for SOS) in granular crystals as a consequence of the small proportion in raw PO despite the higher melting point (Table 2).

According to Ribeiro et al.,[20] the properties of fatty foods can be associated with the TAG composition of the fat they comprise. Wiedermann[21] divided TAGs into four component categories: trisaturated (S_3), disaturated−monounsaturated (S_2U), monosaturated−diunsaturated (SU_2), and triunsaturated (U_3) TAGs. The S_3 TAGs, with melting points from 56.60 to 73.40 °C (Table 2), and some S_2U TAGs, with melting points from 30.50 to 41.20 °C, are the main sources of crystal backbone that provide structure for these samples. These high-melting fractions were also designated "crystallization-inducing TAGs". The SU_2 TAGs, with melting points between 2.50 and 23.00 °C, are important with regard to their sensorial and functionality properties at room temperature. The U_3 TAGs serve to promote pourability and ease of handling at low temperatures. Hence, the higher melting TAGs, such as S_3 SSS, PSS, PPS, and PPP, S_2U SOS and POS in BTMS, S_3 PPP, and S_2U POP and POS in POMS, had occurred gather in granular crystal fractions as the driving force provided by the temperature fluctuation, as observed by the TAGs composition analysis. When the storage temperature is 20 °C, lower melting TAGs will melt into the surrounding material fractions, whereas the higher melting TAGs such as S_3 and S_2U listed above are still in their crystal state. This may have enabled the crystals of these molecules to migrate and agglomerate to form larger crystals. It was, therefore, suggested that higher melting TAGs are one of the key factors for the formation of granular crystals, whether in BTMS or in POMS. On the premise of maintaining a certain SFC, reducing higher melting TAGs will make the TAG composition of base stocks more reasonable. The appropriate proportions of high-melting and low-melting TAGs will avoid migration and agglomeration effects, which will help in the manufacture of shortenings and margarines with reduced tendency to the formation of granular crystals. Thus, it is logical to assume that BT and PO chemically modified, by interesterification with a suitable vegetable oil, or physically modified, by fractionation, plastic products with lower melting points and with no TAG separation problems could be produced, targeting commercial applications.

Thermal Behavior. Thermal profiles obtained by DSC analyses reveal transition temperatures and heats involved in the melting and crystallization processes of fats and oils, providing complementary results to lipid composition data. The melting and crystallization curves of the granular crystals and surrounding

Table 1. Fatty Acid Composition (Percent) of BT, PO, Granular Crystals, and Surrounding Materials in BTMS and POMS[a]

fatty acid	BT	BTMS granular crystals	BTMS surrounding materials	PO	POMS granular crystals	POMS surrounding materials
$C_{12:0}$	0.13 ± 0.01 B	0.12 ± 0.01 C	0.16 ± 0.01 A	0.22 ± 0.01 B	0.21 ± 0.02 B	0.29 ± 0.03 A
$C_{14:0}$	3.21 ± 0.01 B	3.20 ± 0.03 B	3.29 ± 0.02 A	1.11 ± 0.01 B	1.06 ± 0.01 C	1.16 ± 0.02 A
$C_{16:0}$	25.78 ± 0.09 B	26.15 ± 0.11 A	25.25 ± 0.13 C	45.27 ± 0.13 B	48.95 ± 0.16 A	41.62 ± 0.14 C
$C_{16:1}$	3.03 ± 0.02 B	2.88 ± 0.01 C	3.13 ± 0.01 A	0.14 ± 0.01 B	0.07 ± 0.01 C	0.17 ± 0.01 A
$C_{17:0}$	1.61 ± 0.01 A	1.53 ± 0.01 C	1.58 ± 0.01 B	0.08 ± 0.01 B	0.06 ± 0.01 B	0.11 ± 0.01 A
$C_{17:1}$	0.71 ± 0.01 A	0.64 ± 0.01 B	0.67 ± 0.01 B	nd[b]	nd	nd
$C_{18:0}$	20.24 ± 0.05 B	20.67 ± 0.08 A	19.48 ± 0.05 C	4.25 ± 0.03 B	4.38 ± 0.02 A	3.97 ± 0.01 C
$C_{18:1}trans$	3.81 ± 0.01 B	3.70 ± 0.01 C	4.10 ± 0.01 A	nd	nd	nd
$C_{18:1}$	33.78 ± 0.13 A	33.15 ± 0.14 B	33.93 ± 0.09 A	37.12 ± 0.16 B	35.21 ± 0.16 B	38.65 ± 0.15 A
$C_{18:2}trans$	0.11 ± 0.01 A	0.09 ± 0.01 A	0.11 ± 0.01 A	nd	nd	nd
$C_{18:2}$	1.32 ± 0.01 B	1.29 ± 0.01 C	1.48 ± 0.01 A	10.06 ± 0.03 B	7.64 ± 0.02 C	11.98 ± 0.04 A
$C_{20:0}$	0.15 ± 0.01 A	0.14 ± 0.01 A	0.15 ± 0.01 A	0.28 ± 0.01 B	0.28 ± 0.01 B	0.33 ± 0.01 A
$C_{20:1}$	0.05 ± 0.01 A	0.05 ± 0.01 A	0.07 ± 0.01 A	0.15 ± 0.01 B	0.11 ± 0.01 C	0.18 ± 0.01 A
$C_{18:3}\omega3$	0.45 ± 0.01 B	0.42 ± 0.01 C	0.48 ± 0.01 A	0.11 ± 0.01 A	0.09 ± 0.01 B	0.12 ± 0.01 A
others[c]	5.62 ± 0.01 C	5.97 ± 0.01 B	6.12 ± 0.01 A	1.21 ± 0.01 C	1.94 ± 0.01 A	1.42 ± 0.01 B
$\sum$TFA[d]	3.92 ± 0.01 B	3.79 ± 0.01 C	4.21 ± 0.01 A	nd	nd	nd
$\sum$SFA[e]	51.12 ± 0.19 B	51.81 ± 0.23 A	49.91 ± 0.17 C	51.21 ± 0.20 B	54.94 ± 0.25 A	47.48 ± 0.18 C
$\sum$USFA[f]	39.34 ± 0.18 B	38.43 ± 0.15 C	39.76 ± 0.14 A	47.58 ± 0.18 B	43.12 ± 0.14 C	51.10 ± 0.17 A

[a] Values with different letters (A–C) in the same row within the same substrate sample (BT and BTMS, PO and POMS, respectively) are significantly different ($P < 0.05$). [b] nd, not detected. [c] Others, other fatty acids but not identified by the FAME standards. [d] ΣTFA, the sum of trans fatty acids. [e] ΣSFA, the sum of saturated fatty acids. [f] ΣUSFA, the sum of unsaturated fatty acids. ΣUSFA was calculated except trans fatty acids in lipids.

Table 2. TAG Composition and Content (Percent) of BT, PO, Granular Crystals, and Surrounding Materials in BTMS and POMS and Their Melting Points[a]

TAG[b]	BT	BTMS granular crystals	BTMS surrounding materials	% content changes[c]	PO	POMS granular crystals	POMS surrounding materials	% content changes[c]	melting point (°C) β′	β
PLO	5.03 ± 0.19 A	5.01 ± 0.16 A	5.07 ± 0.21 A	−1.18	12.17 ± 0.29 A	4.84 ± 0.10 B	12.36 ± 0.34 A	−60.84		
PLP	nd[d]	nd	nd		10.44 ± 0.21 A	5.18 ± 0.18 B	10.78 ± 0.27 A	−51.95	18.60	
OOO	3.99 ± 0.10 A	3.79 ± 0.09 B	4.05 ± 0.11 A	−6.42	3.12 ± 0.07 A	1.20 ± 0.02 B	3.14 ± 0.08 A	−61.78	−11.80	5.10
POO	21.80 ± 0.52 A	18.09 ± 0.41 B	22.48 ± 0.81 A	−19.53	25.54 ± 0.52 B	16.14 ± 0.66 C	37.72 ± 0.75 A	−57.21	2.50	19.20
POP	14.87 ± 0.39 A	14.24 ± 0.45 B	14.96 ± 0.37 A	−4.81	30.23 ± 0.58 B	62.32 ± 0.94 A	26.50 ± 0.71 C	135.17	30.50	35.30
PPP	6.46 ± 0.13 A	6.57 ± 0.15 A	6.42 ± 0.20 A	2.34	2.68 ± 0.08 A	2.79 ± 0.13 A	2.13 ± 0.09 B	30.99	56.60	66.10
SOO/SSL[e]	6.20 ± 0.12 A	5.19 ± 0.16 B	6.47 ± 0.18 A	−19.78	1.39 ± 0.02 B	0.31 ± 0.01 C	1.50 ± 0.01 A	−79.33	8.60	23.00
POS	15.26 ± 0.48 A	15.41 ± 0.62 A	13.85 ± 0.31 B	11.26	3.96 ± 0.05 A	4.04 ± 0.10 A	2.24 ± 0.09 B	80.36	33.20	38.20
PPS	6.59 ± 0.16 B	7.50 ± 0.21 A	6.24 ± 0.18 B	20.19	0.67 ± 0.01 A	nd	0.26 ± 0.01 B		59.90	62.90
SOS	3.74 ± 0.06 B	4.06 ± 0.09 A	3.11 ± 0.07 C	30.55	0.15 ± 0.01 A	0.03 ± 0.01 C	0.10 ± 0.01 B	−70.00	36.60	41.20
PSS	4.22 ± 0.11 A	4.34 ± 0.16 A	3.77 ± 0.09 B	15.12	nd	nd	nd		60.80	65.00
SSS	0.44 ± 0.01 B	0.61 ± 0.01 A	0.32 ± 0.01 C	90.63	nd	nd	nd		64.10	73.30
others[f]	11.40 ± 0.30 C	15.19 ± 0.41 A	13.26 ± 0.29 B		9.65 ± 0.20 A	3.15 ± 0.11 B	3.27 ± 0.08 B			

[a] Values with different letters (A–C) in the same row within the same substrate sample (BT and BTMS, PO and POMS, respectively) are significantly different ($P < 0.05$). [b] TAG shown constitutes the major species present; P, palmitoyl; L, linoleoyl; O, oleoyl; S, stearoyl. [c] Percent contents changes calculated according to the following formula: % contents changes = $(G - S) \times 100\%/S$, where G refers to content of specific TAG in granular crystals and S refers to content of corresponding TAG in surrounding materials. [d] nd, not detected. [e] TAG SOO/SSL for BT and BTMS, only SOO for PO and POMS; the melting point corresponding to SOO. [f] Others, other TAGs but not identified by HPLC/APCI-MS analysis.

materials obtained from BTMS and POMS, respectively, are presented in Figure 1.

For BTMS, the melting thermogram of granular crystals showed four small endothermic peaks between 3.18 and 31.92 °C and a big sharp endothermic peak (45.23 °C), which slightly moved toward lower temperature in surrounding materials, showing four small endothermic peaks between 0.78 and 28.53 °C and a big sharp endothermic peak (44.24 °C), as illustrated in Figure 1A. The required enthalpy variations (ΔH, J/g) in each peak of the granular crystals were 0.66, 1.72, 0.86, 0.18, and 27.62
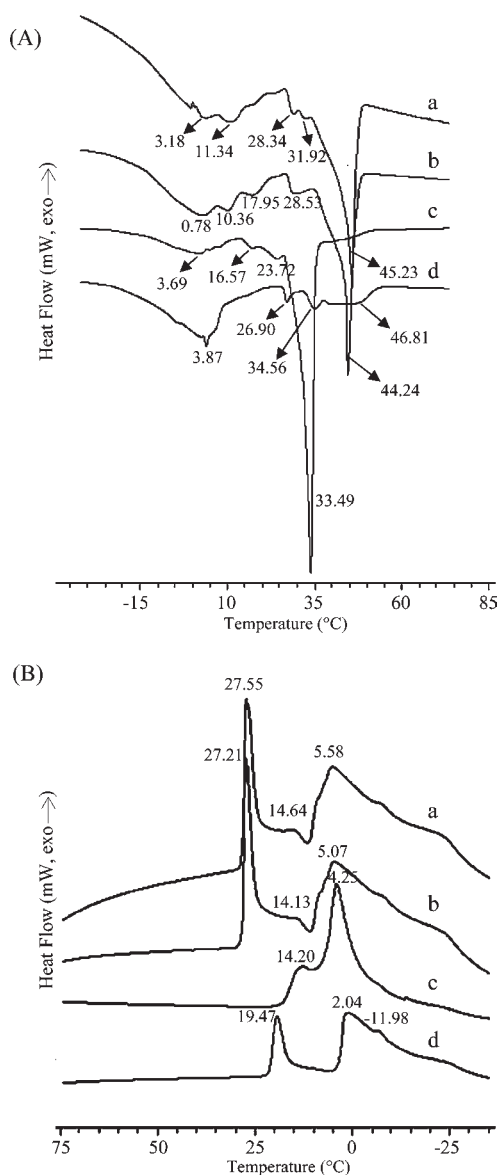
1435

dx.doi.org/10.1021/jf103875f |*J. Agric. Food Chem.* 2011, 59, 1432–1441

Figure 1. DSC melting (A) and crystallization (B) thermograms of granular crystals, surrounding materials in BTMS and POMS. Letters a and c refer to granular crystals separated from BTMS and POMS, respectively; letters b and d refer to surrounding materials separated from BTMS and POMS, respectively.

J/g and those of surrounding materials were 7.87, 1.05, 1.24, 1.86, and 27.56 J/g, respectively. The crystallization curve of granular crystals showed three major exotherms: a sharp high-temperature peak (27.55 °C, ΔH = 15.96 J/g), a small middle-temperature peak (14.64 °C, ΔH = 0.57 J/g), and a broad low-temperature peak (5.58 °C, ΔH = 16.60 J/g). Similarly, the overall crystallization thermogram of surrounding materials shifted slightly to lower temperature (Figure 1B). The corresponding peak temperature shifted to 27.21, 14.13, and 5.07 °C, respectively, and their ΔH values also decreased to 15.04, 0.39, and 15.24 J/g, respectively. These results also indicated that the granular crystals contained a little more total high-melting species and fewer low-melting species than their surrounding materials in BTMS.

For POMS, the melting curve of granular crystals was characterized by a broad low-temperature peak (ΔH = 5.26 J/g), two

small middle-temperature peaks (ΔH = 0.60 and 0.96 J/g, respectively), and a sharp high-temperature peak (ΔH = 55.61 J/g) spreading from 3.69 to 33.49 °C. The big sharp endothermic peak at 33.49 °C consisted of high-melting TAGs that were most likely corresponded to POP (melting point = 35.30 °C in β polymorph). The melting thermogram of the surrounding materials showed four endothermic peaks, namely, a broad peak at 3.87 °C, a small middle-temperature peak at 26.90 °C, a small high-temperature peaks at 34.56 °C, which decreased in size as the amount of POP in the samples decreased, and a broad high-temperature peak at 46.81 °C. Their corresponding ΔH values were 15.13, 1.39, 1.75, and 4.91 J/g, respectively. Meanwhile, the small peak near 16.57 °C disappeared (Figure 1A). The crystallization thermogram of granular crystals showed two not completely separate exothermic peaks at 14.20 and 4.25 °C, corresponding to ΔH = 2.78 and 24.86 J/g, respectively. Their surrounding materials crystallized at a sharp peak at 19.47 °C (ΔH = 9.66 J/g) and a broad peak at 2.04 °C (ΔH = 6.06 J/g) with a shoulder at -11.98 °C (ΔH = 1.23 J/g), which showed broader crystallization temperature range than the granular crystal fractions (Figure 1B). In addition, the ΔH values for surrounding materials were observed to be higher at high crystallization temperature and lower at low crystallization temperature than that of granular crystal fractions (P < 0.05). This means surrounding materials in POMS consisted of slightly higher high-melting and low-melting components, which was in total accordance with TAGs composition data (Table 2).

Polymorphic Behavior. XRD was used to characterize the TAG polymorphic form and the chain packing of fatty acid end groups by determining the short and long spacings of crystals. Three basic polymorphic structures have been recognized, namely, α, β', and β forms, determined on the basis of the characteristic short spacings of crystals previously described. Generally, the TAGs with the same or very similar fatty acids might form a double chain length structure. Unsymmetrical glycerides may give triple chain length. The diffraction peak of long spacing near 41 Å with the (003) reflection near 14 Å indicated the presence of the double chain length structure, whereas the long spacing near 61 Å with the (002) reflection near 31 Å represented the presence of triple chain length structure, although the 61 Å peak might not appear because of limited 2θ angles.[22]

In Figure 2A, the short spacing patterns of 4.6 Å and 4.2 and 3.8 Å appeared in the granular crystals and surrounding materials obtained from both BTMS and POMS, which is characteristic of polymorphic forms β and β', respectively. For BTMS, the granular crystals (Figure 2A, a) showed a relatively higher intensity peak at 4.6 Å than their surrounding materials (Figure 2A, b), corresponding to more of the β form crystal. The granular crystals of POMS (Figure 2A, c) displayed a relatively stronger short spacing peak at 4.6 Å, indicating the predominantly β form crystal, and their surrounding materials (Figure 2A, d) showed low-intensity peaks due to the concomitant presence of a great amount of liquid oil. Table 3 details the polymorphic forms of the granular crystals and surrounding materials obtained from both BTMS and POMS, respectively. For BTMS, both the granular crystals and surrounding materials presented a predominance of polymorphic form β' (69.96 and 87.41%, respectively), although form β was verified in smaller proportions (30.04 and 12.59%, respectively) in both two parts. On the other hand, the surrounding materials of POMS consisted primarily of the β' crystalline form (72.88%), but the main

crystal composed of granular crystals of POMS was the β form (92.74%). These results suggested that parts of the crystal transformed from metastable β' to stable β had occurred in the granular crystals compared with their surrounding materials, whether in BTMS or in POMS. These polymorphic transformations can be associated with the migration and agglomeration of different melting point TAGs in BTMS and POMS as discussed under Lipid Composition. Because an increase in the content of S_3 and S_2U TAGs such as PPP, SSS, and PSS (for BTMS) and PPP and POP (for POMS) (mainly β-tending TAGs), a significant decrease in the content of SU_2 TAGs such as PLO and POO (mainly β'-tending TAGs) had occurred in granular crystal fractions.[23−25]

In Figure 2B, long spacing patterns of 41.3 and 14.3 Å were observed in both granular crystals (Figure 2B, a) and their surrounding materials (Figure 2B, b) obtained from BTMS, which is characterized as a typical double chain length structure. Besides, granular crystals of BTMS had an additional low-intensity diffraction at the long spacing of 32.2 Å (near 31 Å), indicating a mixture of triple chain length and double chain

length structure crystals. Similarly, diffraction peaks of 39.7 and 14.0 Å appeared in both granular crystals (Figure 2B, c) and surrounding materials (Figure 2B, d) of POMS, which is also characteristic of double chain length structure. Additionally, granular crystals of POMS possessed another two long spacing spectra (29.4 and 10.1 Å), both of which correspond to the occurrence of triple chain length structure crystals.

From the results above, we can infer that the formation of granular crystals is associated with the polymorphic transformation in the high-melting fats from β' form of double chain length structures to complicated polymorphic structures, which simultaneously contain the β and β' form crystals of triple chain length and double chain length structures. As discussed by Liu et al.,[11] chemical interesterification of the BT/canola oil blend caused a more balanced rearrangement of TAG species, and the resultant interesterified fat was the exclusively double chain stacking β' crystal. Additionally, some emulsifiers can be used as "crystal structure modifiers" and "polymorphic retardant agents" in plastic fats, because they can crystallize together with TAGs and therefore retard or even prevent polymorphic transformations.[26] Therefore, it suggested that the formation of granular crystals of BT/PO-based plastic fats was related to the polymorphism (phase transformations) of TAGs occurring in the agglomeration in BT and PO. However, the exact manner in which granular crystals on the micrometer scale connected with the TAGs and polymorphisms on the molecular scale was not clear, but the differences in crystallization behavior of granular crystals and surrounding materials might be involved.

Crystallization Kinetics. The crystallization behavior of lipids profoundly influences the final structure of plastic fats and is intrinsically related to their macroscopic properties. The comparative study of crystallization kinetics between granular crystals and surrounding materials separated from BTMS and POMS, respectively, is significant so that fat can be adjusted to product formulas and industrial process limitations, which include base stock design and fat fraction recrystallization, assuring the quality of the final product.[13,27]

Figure 3 shows the increase in SFC with time for the samples crystallized at different temperatures (T_c). Curves obtained for granular crystals (Figure 3C) and surrounding materials (Figure 3D) separated from POMS at 35 °C are not reported here, because of their low SFC in this study at this temperature. For BTMS, the granular crystals (Figure 3A) and their surrounding materials (Figure 3B) crystallized very rapidly at crystallization temperatures below 25 °C, and curves showed two-step primary crystallization; that is, a slight plateau in SFC was clearly visible in all curves. The first step decreased steadily in both rate and height as T_c was increased. The second step of crystallization was sigmoidal in shape. At low supercoolings (T_c above 25 °C), curves showed sigmoidal shapes. That is, there appeared an initial lag period during which no fat crystallized, followed by a period of rapid crystallization. These curves displayed the existence of two distinct crystallization mechanism regions, one below and the other above 25 °C. The division between these two regions
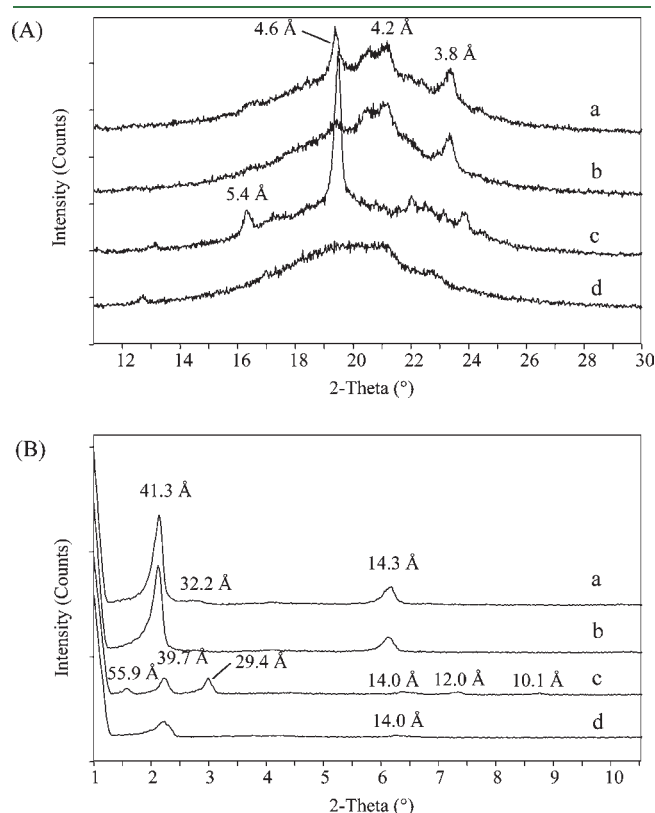
Figure 2. Diffractograms for short (A) and long (B) spacings of granular crystals, surrounding materials in BTMS and POMS determined by XRD. Letters a and c refer to granular crystals separated from BTMS and POMS, respectively; letters b and d refer to surrounding materials separated from BTMS and POMS, respectively.

Table 3. Polymorphic Forms (Percent) of Granular Crystals and Surrounding Materials in BTMS and POMS

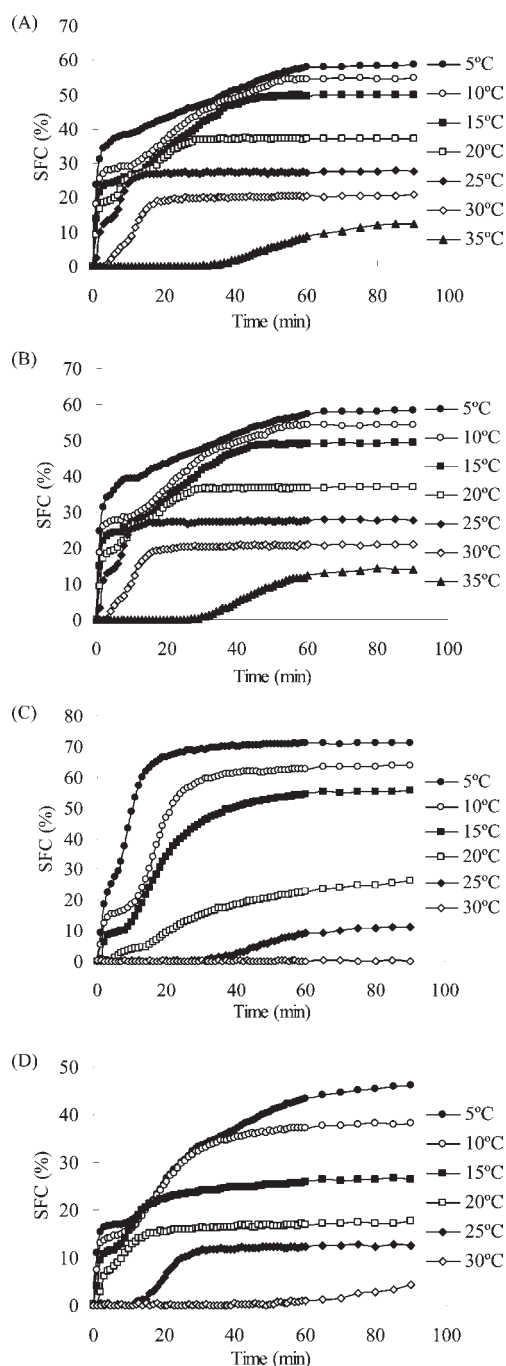|	BTMS		POMS	
polymorphic form	granular crystals	surrounding materials	granular crystals	surrounding materials
β	30.04 ± 0.16	12.59 ± 0.11	92.74 ± 0.87	27.12 ± 0.20
β'	69.96 ± 0.58	87.41 ± 0.91	7.26 ± 0.10	72.88 ± 0.69

Figure 3. SFC versus time of crystallization for granular crystals and surrounding materials in BTMS and POMS at 5, 10, 15, 20, 25, 30, and 35 °C: (A, C) granular crystals separated from BTMS and POMS, respectively; (B, D) surrounding materials separated from BTMS and POMS, respectively.

was very noticeable. Similarly, two different regions were also determined in granular crystals (Figure 3C) and surrounding materials (Figure 3D) separated from POMS, below and above 20 °C. Below 20 °C, crystallization showed hyperbolic patterns against time, and an equilibrium value in SFC was clearly visible in all curves, especially for granular crystals, which crystallized more rapidly at each corresponding temperature. For the T_c above 20 °C, curves had sigmoidal shapes. PO is known to exhibit a two-step crystallization below a certain critical temperature,

which depends on composition.[28] Given this argument, it was not surprising that in granular crystals (Figure 3C) and surrounding materials (Figure 3D) separated from POMS below 20 °C, similar to the foregoing discussion of the two parts in BTMS, crystallization curves also appeared to be two-step crystallization processes. Generally, a two-step primary crystallization mechanism can be due to a fractionated crystallization, a polymorphic transformation, or a combination thereof. According to the TAG composition (Table 2) and polymorphic form (Table 3) data previously discussed, this two-step mechanism appeared to be caused by a fractionated crystallization into high-melting and low-melting fractions; possibly, all four fats undergo a β' mediated β crystallization. This suggested that higher melting fractions began to crystallize first, later joined by the lower melting fractions. Meanwhile, SFC versus time profiles are also sensitive to both the formation and transformation of the various polymorphic forms, as has been demonstrated in the study by Marangoni et al.[29]

Avrami Analysis. The Avrami model is the one most prevalently used to study the crystallization of fats and may be used to evaluate the crystallization kinetics and suggest the nature of crystal growth. To quantify differences in the crystallization behaviors of granular crystals and surrounding materials separated from BTMS and POMS, respectively, the SFC crystallization kinetic data were fitted separately by Avrami equations. The equation fitted the data very well over the entire range of fractional crystallization shown in Table 4 ($R^2 > 0.99$ in all cases) except crystallization curves at 30 °C for granular crystals and surrounding materials separated from POMS, which were not included because crystallization kinetics were too slow to give a good fit (curves in Figure 3C,D). The Avrami exponent (n), Avrami constant (K), and half-times of crystallization ($t_{1/2}$) determined from the curve fits are also shown in Table 4.

Not surprisingly, K values were higher at lower temperatures ($P < 0.001$), indicating that crystallization proceeded more rapidly at a higher degree of supercooling (lower T_c). In granular crystals and surrounding materials separated from BTMS at 30 and 35 °C, crystallization temperature had a very strong influence on K ($P < 0.001$), which dropped by factors of roughly 10 and 10^7 (for granular crystals) and 10^2 and 10^6 (for surrounding materials) compared to the values at 25 °C, respectively. For granular crystals and surrounding materials separated from POMS, this behavior was also shown, but 20 °C was the critical temperature that distinguished the two regions. Correspondingly, the K values dropped by a factor of roughly 10^6 and 10^5 ($P < 0.001$), respectively, when the crystallization temperature was above 20 °C. The declining K values also indicated a change in the nucleation and/or growth rate in granular crystals and surrounding materials, whether in BTMS or in POMS, below and above the critical temperatures noted above. Because K is a combined function of nucleation and growth as well as a strong function of temperature, the declines ineluctably induce changes in crystal morphology, such as crystal size, type, and so on. The increase in $t_{1/2}$ for the four fats as a function of increasing crystallization temperature also reflected the decrease in K at higher temperatures. For BTMS, by comparison of the K and $t_{1/2}$ of the granular crystals and surrounding materials at each crystallization temperature, it can be found that the former had lower K values and higher $t_{1/2}$ values ($P < 0.05$). For POMS, slower crystallization of granular crystals was also evidenced by the decrease in the parameter K and the increase in $t_{1/2}$ compared with their surrounding materials at the same supercoolings ($P < 0.05$).

Table 4. Avrami Exponent (n), Avrami Constant (K), and Half-Time of Crystallization ($t_{1/2}$) for Granular Crystals and Surrounding Materials Separated from BTMS and POMS, Respectively, at Different Crystallization Temperatures[a]

sample	temperature (°C)	n	K (min^{-n})	$t_{1/2}$ (min)	R^2
BTMS					
granular crystals	5	0.248 ± 0.011	0.641 ± 0.031	1.373 ± 0.051	0.999
	10	0.497 ± 0.010	0.413 ± 0.029	2.833 ± 0.173	0.994
	15	0.640 ± 0.022	0.332 ± 0.012	3.158 ± 0.092	0.993
	20	0.700 ± 0.034	0.286 ± 0.008	3.534 ± 0.202	0.996
	25	1.218 ± 0.037	0.091 ± 0.009	5.291 ± 0.518	0.998
	30	2.447 ± 0.053	$0.002 \pm 1.01 \times 10^{-4}$	10.901 ± 0.626	0.992
	35	4.815 ± 0.115	$3.47 \times 10^{-9} \pm 1.65 \times 10^{-10}$	52.962 ± 1.382	0.993
surrounding materials	5	0.237 ± 0.009	0.651 ± 0.030	1.297 ± 0.046	0.999
	10	0.451 ± 0.016	0.437 ± 0.031	2.776 ± 0.181	0.995
	15	0.541 ± 0.011	0.372 ± 0.015	3.157 ± 0.197	0.998
	20	0.679 ± 0.019	0.303 ± 0.010	3.387 ± 0.211	0.996
	25	1.108 ± 0.035	0.126 ± 0.009	4.673 ± 0.475	0.995
	30	2.226 ± 0.047	$0.005 \pm 1.04 \times 10^{-4}$	9.244 ± 0.568	0.997
	35	3.949 ± 0.108	$2.15 \times 10^{-7} \pm 1.38 \times 10^{-8}$	44.462 ± 1.404	0.994
POMS					
granular crystals	5	1.691 ± 0.032	0.024 ± 0.002	7.372 ± 0.482	0.992
	10	1.718 ± 0.051	$0.007 \pm 1.11 \times 10^{-4}$	14.124 ± 0.615	0.999
	15	1.729 ± 0.048	$0.005 \pm 1.02 \times 10^{-4}$	17.118 ± 0.537	0.996
	20	1.736 ± 0.063	$0.002 \pm 1.07 \times 10^{-4}$	26.788 ± 0.771	0.993
	25	4.756 ± 0.132	$6.05 \times 10^{-9} \pm 2.59 \times 10^{-10}$	49.507 ± 1.054	0.994
surrounding materials	5	0.467 ± 0.014	0.276 ± 0.019	7.181 ± 0.416	0.996
	10	0.913 ± 0.036	0.110 ± 0.007	7.498 ± 0.375	0.994
	15	0.965 ± 0.029	0.099 ± 0.003	7.525 ± 0.428	0.993
	20	1.190 ± 0.037	0.036 ± 0.001	12.083 ± 0.613	0.995
	25	4.612 ± 0.125	$5.95 \times 10^{-7} \pm 1.84 \times 10^{-8}$	20.670 ± 0.784	0.996

[a] Values that differ by more than 10% are significantly different at $P < 0.05$ within either n, K, or $t_{1/2}$ columns.

These indicated that granular crystals showed slower crystallization rate at all crystallization temperatures, whether in BTMS or in POMS. Meanwhile, at the same crystallization temperatures, values of K were higher for the fat samples separated from BTMS and lower for the samples separated from POMS, and the opposite was observed for $t_{1/2}$ values ($P < 0.05$), which were in agreement with the poor crystallization properties of palm oil, that is, the low rate of nucleation and crystal growth.

n is a function of the number of dimensions in which growth takes place and reflects the details of nucleation and growth mechanisms. Cheong et al.[30] has tabulated values of n for various types of nucleation and growth. For example, an n of 4 indicates heterogeneous nucleation and spherulitic growth from sporadic nuclei, whereas an n of 3 corresponds to spherulitic growth from instantaneous nuclei or disk-like growth from sporadic nuclei; an n of 2 denotes rod-like growth from sporadic nuclei or disk-like growth from instantaneous nuclei, and an n of 1 represents rod-like growth from instantaneous nuclei. For the granular crystals and surrounding materials individually, whether in BTMS or in POMS, an increase in n from ~1 to ~4 with increasing temperature could also be due to a change in the type of nucleation and growth, from more rod-like growth from instantaneous nuclei at higher degrees of supercooling to more spherulitic growth from sporadic nuclei at lower degrees of supercooling. Meanwhile, n increased significantly above 25 °C for fat samples separated from BTMS and above 20 °C for

samples separated from POMS. Correspondingly, these were the same points at which the greatest change in K occurred. According to the Avrami analysis, two different crystallization mechanisms would be expected below and above the critical temperatures noted above on the basis of the differences in n values. Additionally, as shown in Table 4, values of n were higher for granular crystals and lower for their surrounding materials, whether in BTMS or in POMS, and the opposite trend was observed for K values ($P < 0.05$), at all the same supercoolings. Generally, low values of n and high values of K are associated with an increased rate of crystallization and a more instantaneous nucleation process with a shorter induction time. This, in turn, would yield smaller and more numerous crystals. The opposite would also be true for granular crystals, namely, the formation of larger and fewer crystals, whether in BTMS or in POMS. As previously discussed, some emulsifiers have been employed as a crystallization controller, revealing the effects of inhibition of crystal growth resulting in small crystal sizes.[26]

In the present study, it was found that the migration and aggregation of higher melting TAGs, such as S_3 SSS, PSS, PPS, and PPP and S_2U SOS and POS in BTMS and S_3 PPP and S_2U POP and POS in POMS. Consequently, polymorphic transformation from β' form of double chain length structures to complicated crystal structures, concurrently comprising the β and β' form crystals of triple chain length and double chain length structures, had occurred in granular crystal parts as the driving force provided

by the temperature fluctuation. These changes of nanostructure occasioning the sample crystallization rate declined and were accompanied by an increase in crystal sizes. The crystals of high-melting TAGs, which were still in their crystal state, were aggregated and then continued to grow larger through further crystallization, leading to the formation of large granular crystals, whether in BTMS or in POMS. Accordingly, it was suggested that possible techniques to prevent the formation of the granular crystals may be developed by paying attention to the high-melting TAGs and the growth and aggregation of crystals. BT/PO interesterified with a suitable vegetable oil or directly by fractionation to lower high-melting TAGs of base stocks, making their TAG composition more reasonable, is under investigation. Additionally, emulsifiers have been employed as crystallization controllers and polymorphic retardant agents to inhibit the crystal growth and retard the polymorphic transformation.

■ ABBREVIATIONS USED

BT, beef tallow; PO, palm oil; BTMS, all beef tallow-based model shortenings; POMS, all palm oil-based model shortenings; TAGs, triacylglycerols; POP, 1,3-dipalmitoyl-2-oleoylglycerol; PPP, tripalmitin; RBD, refined, bleached, and deodorized; IV, iodine value; SMP, slip melting point; DSC, differential scanning calorimetry; XRD, X-ray diffraction; pNMR, pulsed nuclear magnetic resonance; FAMEs, fatty acid methyl esters; GC, gas chromatography; HPLC, high-performance liquid chromatography; ELSD, evaporative light scattering detector; HPLC/APCI-MS, high-performance liquid chromatography—atmospheric pressure chemical ionization mass spectrometry; SFC, solid fat content; ANOVA, analysis of variance; ΣSFA, the sum of saturated fatty acids; ΣUSFA, the sum of unsaturated fatty acids; ΣTFA, the sum of trans fatty acids; S_3, trisaturated; S_2U, disaturated—monounsaturated; SU_2, monosaturated—diunsaturated; U_3, triunsaturated; ΔH, enthalpy variation; T_c, crystallization temperature; n, Avrami exponent; K, Avrami constant; $t_{1/2}$, half-time of crystallization.

■ AUTHOR INFORMATION

Corresponding Author
*Phone: (086)510-85876799; fax: (086)510-85876799; e-mail: wxg1002@hotmail.com

■ ACKNOWLEDGMENT

■ REFERENCES

(1) Jin, Q. Z.; Gao, H. Y.; Shan, L.; Liu, Y. F.; Wang, X. G. Study on grainy crystals in edible beef tallow shortening. *Food Res. Int.* **2007**, *40*, 909–914.

(2) Meng, Z.; Liu, Y. F.; Jin, Q. Z.; Huang, J. H.; Song, Z. H.; Wang, F. Y.; Wang, X. G. Characterization of graininess formed in all beef tallow-based shortening. *J. Agric. Food Chem.* **2010**, *58*, 11463–11470.

(3) Ishikawa, H.; Mizuguchi, T.; Kondo, S. Studies on granular crystals growing in palm oil. *J. Jpn. Oil Chem. Soc.* **1980**, *29*, 235–242.

(4) Watanabe, A.; Tashima, I.; Matsuzaki, N.; Kurashige, J.; Sato, K. On the formation of granular crystals in fat blends containing palm oil. *J. Am. Oil Chem. Soc.* **1992**, *69*, 1077–1080.

(5) Miura, S.; Konishi, H. Crystallization behavior of 1,3-dipalmitoyl-2-oleoyl-glycerol and 1-palmitoyl-2,3-dioleoyl-glycerol. *Eur. J. Lipid Sci. Technol.* **2001**, *103*, 804–809.

(6) Tanaka, L.; Isogai, T.; Miura, S.; Murakami, M. Effect of triacylglycerol species on the crystallizing behavior of a model water/oil emulsion. *Eur. J. Lipid Sci. Technol.* **2010**, *112*, 304–309.

(7) Tanaka, L.; Miura, S.; Yoshioka, T. Formation of granular crystals in margarine with excess amount of palm oil. *J. Am. Oil Chem. Soc.* **2007**, *84*, 421–426.

(8) AOCS. *Official Methods and Recommended Practices of the American Oil Chemists' Society*, 5th ed.; American Oil Chemists' Society: Champaign, IL, 1998.

(9) Braipson-Danthine, S.; Deroanne, C. Determination of solid fat content (SFC) of binary fat blends and use of these data to predict SFC of selected ternary fat blends containing low-erucic rapeseed oil. *J. Am. Oil Chem. Soc.* **2006**, *83*, 571–581.

(10) Braipson-Danthine, S.; Deroanne, C. Influence of SFC, microstructure and polymorphism on texture (hardness) of binary blends of fats involved in the preparation of industrial shortenings. *Food Res. Int.* **2004**, *37*, 941–948.

(11) Liu, Y. F.; Meng, Z.; Shan, L.; Jin, Q. Z.; Wang, X. G. Preparation of specialty fats from beef tallow and canola oil by chemical interesterification: physico-chemical properties and bread applications of the products. *Eur. Food Res. Technol.* **2010**, *230*, 457–466.

(12) Chen, C. W.; Chong, C. L.; Ghazali, H. M.; Lai, O. M. Interpretation of triacylglycerol profiles of palm oil, palm kernel oil and their binary blends. *Food Chem.* **2007**, *100*, 178–191.

(13) Ribeiro, A. P. B.; Basso, R. C.; Grimaldi, R.; Gioielli, L. A.; dos Santos, A. O.; Cardoso, L. P.; Gonçalves, L. A. G. Influence of chemical interesterification on thermal behavior, microstructure, polymorphism and crystallization properties of canola oil and fully hydrogenated cottonseed oil blends. *Food Res. Int.* **2009**, *42*, 1153–1162.

(14) Singh, A. P.; Bertoli, C.; Rousset, P. R.; Marangoni, A. G. Matching avrami indices achieves similar hardness in palm oil-based fats. *J. Agric. Food Chem.* **2004**, *52*, 1551–1557.

(15) Raw materials. In *Fats and Oils—Formulating and Processing for Applications*, 3rd ed.; O'Brien, R. D., Ed.; CRC Press: Boca Raton, FL, 2009; pp 1—72.

(16) Vereecken, J.; Foubert, I.; Smith, K. W.; Dewettinck, K. Relationship between crystallization behavior, microstructure, and macroscopic properties in trans-containing and trans-free filling fats and fillings. *J. Agric. Food Chem.* **2007**, *55*, 7793–7801.

(17) Hidalgo, F. J.; Zamora, R. Fats: physical properties. In *Handbook of Food Science, Technology, And Engineering*; Hui, Y. H., Ed.; CRC Taylor & Francis: Boca Raton, FL, 2006; Vol. 1, pp 142—168.

(18) Deman, J. M. Functionality of palm oil in foods. *J. Food Lipids* **1998**, *5*, 159–170.

(19) Lin, S. W. Palm oil. In *Vegetable Oils in Food Technology: Composition, Properties and Uses*; Gunstone, F. D., Ed.; Blackwell Publishing: Oxford, U.K., 2002; pp 59—97.

(20) Ribeiro, A. P. B.; Grimaldi, R.; Gioielli, L. A.; Gonçalves, L. A. G. Zero trans fats from soybean oil and fully hydrogenated soybean oil: physico-chemical properties and food applications. *Food Res. Int.* **2009**, *42*, 401–410.

(21) Wiedermann, L. H. Margarine and margarine oil, formulation and control. *J. Am. Oil Chem. Soc.* **1978**, *55*, 823–829.

(22) Campbell, S. D.; Goff, H. D.; Rousseau, D. Comparison of crystallization properties of a palm stearin/canola oil blend and lard in bulk and emulsified form. *Food Res. Int.* **2002**, *35*, 935–944.

(23) Ribeiro, A. P. B.; Basso, R. C.; Grimaldi, R.; Gioielli, L. A.; Gonçalves, L. A. G. Instrumental methods for the evaluation of interesterified fats. *Food Anal. Methods* **2009**, *2*, 282–302.

(24) Shin, J.-A.; Akoh, C. C.; Lee, K.-T. Production and physico-chemical properties of functional-butterfat through enzymatic interesterification in a continuous reactor. *J. Agric. Food Chem.* **2009**, *57*, 888–900.

(25) Rousseau, D.; Hodge, S.; Nickerson, M.; Paulson, A. Regulating the $\beta' \rightarrow \beta$ polymorphic transition in food fats. *J. Am. Oil Chem. Soc.* **2005**, *82*, 7–12.

(26) Garbolino, C.; Bartoccini, M.; Flöter, E. The influence of emulsifiers on the crystallisation behaviour of a palm oil-based blend. *Eur. J. Lipid Sci. Technol.* **2005**, *107*, 616–626.

(27) Wassell, P.; Young, N. W. G. Food applications of trans fatty acid substitutes. *Int. J. Food Sci. Technol.* **2007**, *42*, 503–517.

(28) De Graef, V.; Foubert, I.; Smith, K. W.; Cain, F. W.; Dewettinck, K. Crystallization behavior and texture of trans-containing and trans-free palm oil based confectionery fats. *J. Agric. Food Chem.* **2007**, *55*, 10258–10265.

(29) Marangoni, A. G.; McGauley, S. E. Relationship between crystallization behavior and structure in cocoa butter. *Cryst. Growth Des.* **2002**, *3*, 95–108.

(30) Cheong, L.-Z.; Zhang, H.; Xu, Y.; Xu, X. Physical characterization of lard partial acylglycerols and their effects on melting and crystallization properties of blends with rapeseed oil. *J. Agric. Food Chem.* **2009**, *57*, 5020–5027.